

## Biomedical Paper

# Real-Time Optical Coherence Tomography for Minimally Invasive Imaging of Prostate Ablation

Stephen A. Boppart, M.D., Ph.D., Juergen M. Herrmann, Ph.D., Costas Pitris, Ph.D., Debra L. Stamper, Ph.D., Mark E. Brezinski, M.D., Ph.D., and James G. Fujimoto, Ph.D. *Research Laboratory of Electronics, Department of Electrical Engineering and Computer Science, Massachusetts Institute of Technology, Cambridge, Massachusetts (S.A.B., J.M.H., C.P., J.G.F.); Harvard-MIT Division of Health Sciences and Technology (S.A.B., C.P.) and Cardiac Unit, Massachusetts General Hospital (M.E.B.), Harvard Medical School, Boston, Massachusetts; and Department of Biology, King's College, Wilkes-Barre, Pennsylvania (D.L.S.)*

**ABSTRACT** Objective: Numerous ablation techniques have been developed to alleviate urethral obstruction and improve urodynamics in benign prostatic hyperplasia. Most techniques, however, rely on visual observation of surface changes for ablation end points. The feasibility of using real-time optical coherence tomography (OCT) for minimally invasive imaging to guide and monitor prostate resection is demonstrated with representative techniques of laser and radiofrequency ablation. Empiric comparisons of ablation dynamics are made, and the use of OCT as a high-resolution, subsurface modality for image guidance is evaluated.

**Materials and Methods:** Optical coherence tomography is a high-resolution, high-speed near-infrared imaging technique analogous to ultrasound imaging, except that reflections of light are detected rather than sound. High-speed OCT is used to image the dynamic process of laser and radiofrequency ablation of *in vitro* human prostate tissue. OCT images of ablation sites are compared with corresponding histology.

**Results:** Based on comparisons between OCT images and corresponding histology, OCT imaged transurethral prostate tissue morphology, including urethral sinuses and submucosal glands. Real-time OCT imaging provided rapid feedback and control of ablation dynamics. The compact and portable OCT technology is amenable to minimally invasive beam-delivery devices.

**Conclusions:** Optical coherence tomography offers a minimally invasive means of assessing transurethral prostate morphology. Real-time OCT has the potential to provide image guidance of prostate resection for many of the existing surgical treatments directed at alleviating urethral obstruction associated with benign prostatic hyperplasia. *Comp Aid Surg* 6:94-103 (2001). ©2001 Wiley-Liss, Inc.

---

**Key words:** TURP, TUNA, BPH, optical coherence tomography (OCT), imaging

---

## INTRODUCTION

Transurethral resection of the prostate (TURP) was the first major endoscopic operative procedure in medicine, and is currently the gold standard for the surgical treatment of BPH against which all other

treatments are evaluated.<sup>1-3</sup> However, high postoperative morbidity and reoperation rates have prompted the investigation of other resection techniques that utilize focused ultrasound,<sup>4,5</sup> micro-

---

Received April 11, 2000; accepted February 13, 2001.

Address correspondence/reprint requests to: James G. Fujimoto, Ph.D., Department of Electrical Engineering and Computer Science, Research Laboratory of Electronics, Massachusetts Institute of Technology, 77 Massachusetts Ave., Room 36-345, Cambridge, MA 02139.

©2001 Wiley-Liss, Inc.

waves,<sup>6,7</sup> laser radiation,<sup>8,9</sup> or radiofrequency energy.<sup>10,11</sup> The morbidity factors of TURP and other prostate resection procedures can be attributed, in part, to poor or ineffective visualization and dosimetry during the resection process. Hence, image-guidance technologies are important. Endoscopy and fiber optics have been used to position instruments and monitor ablation, but only surface features can be visualized. Transrectal ultrasound and MRI have been used to monitor the extent of thermal ablation within the prostate. Image resolution, however, is on the order of hundreds of microns, often leading to inaccurate lesion-diameter estimations.<sup>12,13</sup> Improved imaging techniques for monitoring and dosimetry have the potential to improve the outcomes of many of the existing surgical treatments. The use of a high-resolution, real-time technology capable of imaging transurethral subsurface tissue morphology and guiding ablation would enable improved localization and resection, with the potential to reduce iatrogenic injury during prostate resection.

Optical coherence tomography (OCT) is an emerging minimally invasive optical imaging technology.<sup>14–16</sup> The OCT technology has a number of features that make it attractive and able to be engineered for ultimate clinical applications, such as high-speed surgical guidance at micron-scale resolutions.<sup>14,15</sup> Because OCT is based on fiber-optic technology, it draws upon a well-developed optical communications technology base. OCT can be easily interfaced to surgical microscopes,<sup>17</sup> endoscopes,<sup>18</sup> laparoscopes,<sup>19</sup> catheters,<sup>20</sup> and handheld probes<sup>19</sup> where, in contrast to ultrasound, no active transducer is required near the tissue and imaging can be performed with small optical fibers. Unlike technologies such as MRI or CT, OCT can be engineered into a compact, portable, and relatively inexpensive instrument, allowing wider accessibility. Recently, OCT has been applied to imaging highly scattering tissues,<sup>21,22</sup> for use in surgical guidance,<sup>14</sup> and for *in vivo* imaging of the gastrointestinal tract in animal models and humans.<sup>18,23,24</sup>

A previous OCT imaging survey of *in vitro* urinary tract tissue demonstrated that OCT resolutions are sufficient to image prostatic morphology and neurovascular bundles.<sup>25</sup> The objective of this *in vitro* study is to demonstrate the feasibility of high-speed OCT for real-time minimally invasive imaging of prostate ablation and vaporization during radiofrequency (RF) and laser ablation. The use of real-time OCT for the dosimetric monitoring of prostate resection has the potential to provide im-

age guidance for a large number of existing minimally invasive surgical techniques.

## MATERIALS AND METHODS

Optical coherence tomography is a medical diagnostic imaging technology that permits the *in situ*, micron-scale, tomographic cross-sectional imaging of microstructures in biological tissues. OCT imaging is somewhat analogous to ultrasound B-mode imaging, except that OCT imaging is performed by measuring the intensity of reflected or backscattered light rather than acoustical waves. OCT is based on a technique known as low-coherence interferometry, which was previously applied in optical communications as well as in biological systems to perform optical ranging with micrometer resolution.<sup>26,27</sup> Figure 1 shows a schematic of the OCT imaging and ablation setup. The OCT instrument used in this study is a laboratory prototype constructed from readily available optical components. Measurements are performed using a fiber-optic Michelson interferometer (fiber coupler, Gould Electronics, Inc., Millersville, MD) with a low-coherence-length light source (amplified superluminescent diode, AFC Technologies, Inc., Canada). Fiber-optic implementation provides a compact and low-cost system that can easily be interfaced to a variety of clinical instruments. Low-coherence light can be generated by a compact superluminescent semiconductor diode or a source such as a femtosecond solid-state laser. One arm of the interferometer is a modular beam-delivery instrument that directs the light onto the sample and collects the retroreflected signal. For this study, a stereo microscope with a pair of integrated galvanometers (Cambridge Technologies, Inc., Cambridge, MA) was used to direct the OCT beam onto the tissue for imaging. An argon laser beam, controlled with a timed mechanical shutter, was coincident with the OCT imaging beam to perform laser ablation. RF energy was delivered to the tissue via a catheter. The reference arm of the OCT instrument includes a mechanism for varying the optical path-length difference between the two arms. This is commonly performed with an optical delay line. Optical interference between the light from the sample and reference mirror occurs only when the optical distances traveled by the light in both the tissue sample and reference paths match to within the coherence length of the light.

Although the penetration of OCT imaging in nontransparent tissue is limited to a few millimeters, the typical image resolution of OCT is 10–15  $\mu\text{m}$ , 10–15 times greater than clinical ultrasound,

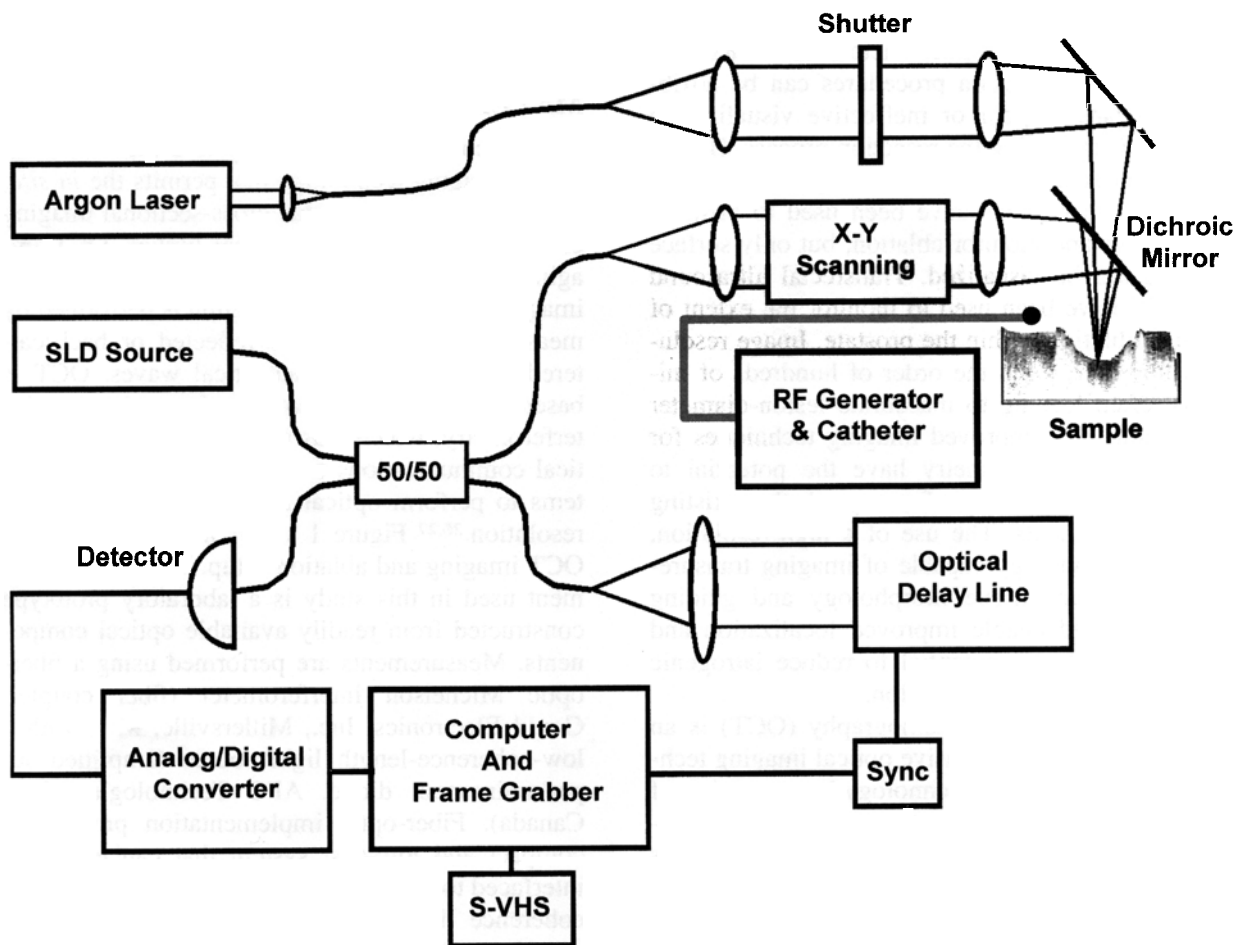


**Fig. 1.** OCT and ablation setup schematic. A fiber-optic coupler equally splits the output of the superluminescent diode (SLD) source into the reference and sample arms of the interferometer. The reference arm contains a high-speed optical delay line which is synchronized by the computer to the frame grabber. The sample arm contains an X-Y scanning mechanism to direct the OCT imaging beam onto the tissue. An argon laser and a radiofrequency catheter are used to ablate prostate tissue under OCT image guidance.

MRI, or CT. OCT imaging with resolutions as high as 1–2  $\mu\text{m}$  is possible with state-of-the-art laboratory-based systems.<sup>28,29</sup> The extremely high sensitivity of OCT allows signal-to-noise ratios in excess of 100 dB, corresponding to the detection of reflected optical signals of 1 part in  $10^{10}$ .

High-speed OCT image acquisition is essential for *in vivo* imaging. Slow acquisition rates are often plagued by motion artifacts from either the operator or the subject. An amplified superluminescent diode was used as a low-coherence light source. This source operates at 1310 nm center wavelength with a coherence length (axial resolution) of 18  $\mu\text{m}$ , and can deliver 5 mW of incident power onto the specimen—sufficient for real-time imaging rates. High-speed axial scanning was performed using an optical delay line based on fem-

tosecond pulse-shaping techniques. Using this optical delay line, axial scans in excess of a few millimeters may be produced at repetition rates of 2000 Hz. These rates enable acquisition of 500 or 250 transverse pixel images at four to eight frames per second. A modified surgical microscope was used to deliver the near-infrared (1310 nm) OCT imaging beam to a 30  $\mu\text{m}$ -diameter spot (transverse resolution) on the tissue. The near-infrared imaging beam is invisible to the human eye. Therefore, to visualize the beam location, a visible beam from a helium:neon laser (632 nm) was implemented as a collinearly aligned aiming beam. Beam scanning across the stationary specimens was performed using a galvanometer-controlled mirror (Fig. 1).

A cadaveric prostate specimen was obtained, maintained in 0.9% saline solution, and imaged

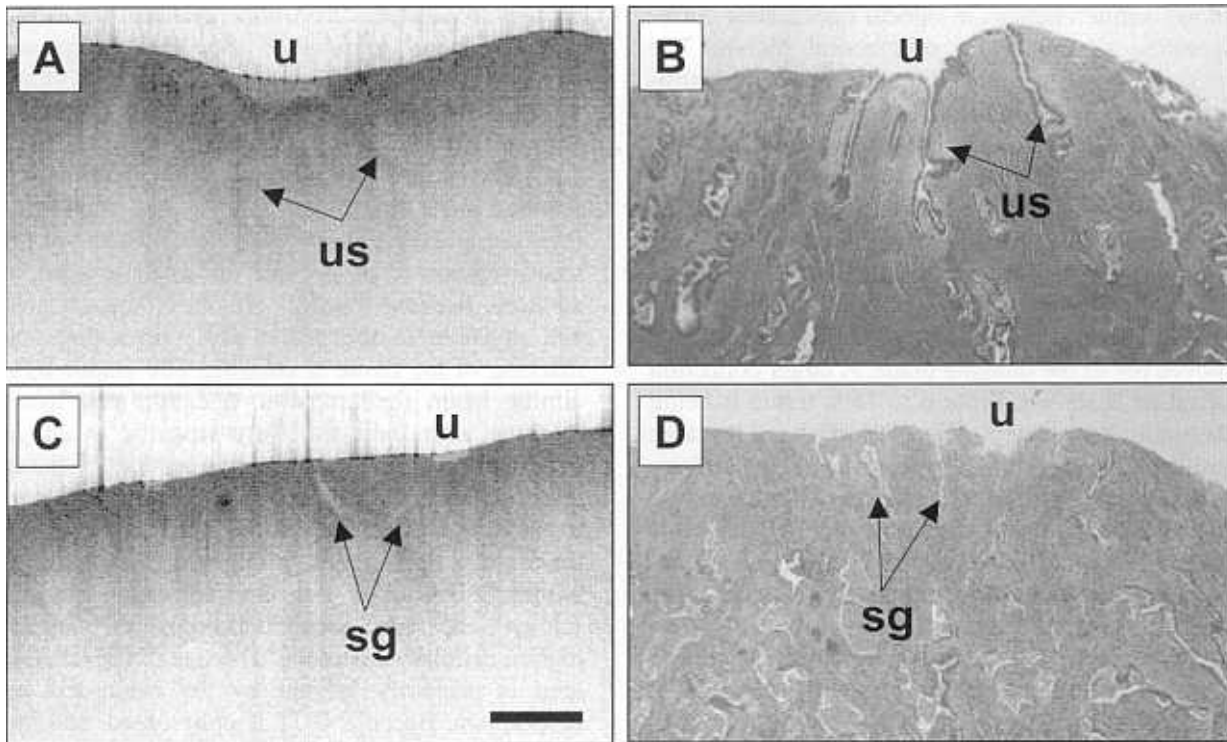


**Fig. 2.** OCT image and corresponding histology of human prostate. *In vitro* human prostate images acquired by hemi-secting the prostate through the urethra (u) and imaging perpendicular to the longitudinal axis of the exposed urethra. (A, B) OCT image and histology illustrating urethral sinuses (us). (C, D) OCT image and histology illustrating submucosal glands (sg). Bar represents 500  $\mu\text{m}$ .

within 24 h of death. The *in vitro* specimen was hemi-sected through the urethra and placed in the OCT setup for RF and argon laser ablation. Laser radiation from an argon laser (514 nm wavelength) was delivered through a dichroic beam splitter (reflecting the OCT beam and transmitting the argon laser beam) and focused on the specimen in the image plane of the OCT microscope. The argon beam was focused to a 900  $\mu\text{m}$ -diameter spot, centered within the OCT scan range. For RF ablation studies, an RF ablation catheter with a 3-mm tip was positioned on the specimen, centered with—but lying just outside of—the OCT imaging plane. A grounding electrode was placed in the surrounding tissue bath. An RF power of 2 W was delivered to the specimen for 15 s while OCT imaging at four frames per second was performed. On the second hemi-sected specimen, argon laser ablation using 2 W delivered for 8 s was performed while simultaneously imaging at eight frames per second. Following imaging, the ablation sites were marked using India ink and the specimens were placed in formalin for standard histological processing. Histology sections, 5  $\mu\text{m}$  thick, were

stained with hematoxylin and eosin for light microscopy observation. Comparisons and associations were made between acquired OCT images and corresponding histological preparations. The research protocols in this study involving the use of discarded human tissue have been approved by the MIT Committee on the Use of Humans as Experimental Subjects and the Massachusetts General Hospital.

## RESULTS

To determine which microstructural features of the prostate are resolvable using OCT, images and corresponding histology of a hemi-sected *in vitro* human prostate specimen were acquired. These results are shown in Figure 2. In Figure 2(A), the OCT image ( $3 \times 2$  mm,  $300 \times 450$  pixels) shows the urethra with a collection of saline. Surrounding the urethra are saline-filled urethral sinuses. The corresponding histology shown in Figure 2(B) reveals good association of the prostate morphology. The OCT image and histology shown in Figures 2(C) and (D), respectively, were acquired from a second site on the specimen. The OCT image

shows subtle changes in optical backscatter corresponding to fluid-filled submucosal glands. The presence of these glands is confirmed with histology shown in Figure 2(D).

An OCT image and video sequence of RF prostate ablation is shown in Figure 3. These  $6 \times 3$ -mm,  $512 \times 256$ -pixel images were each acquired in 250 ms (four frames per second). The initial image shows urethral sinuses (arrows) of the hemisectioned urethra filled with collections of saline. After 4 s, the tissue has constricted and portions have moved out of the imaging plane. A larger collection of saline is shown. From 6 to 11 s, tissue is being thermally coagulated at the lesion site. The large lesion site is shown at 15 s (arrows). The histology reveals excellent correspondence, demonstrating a region of coagulated tissue consistent with what was observed in the final OCT image of the sequence. The thermally coagulated tissue is more evident along the right side of the lesion.

Real-time OCT video imaging of argon laser ablation and vaporization is shown in Figure 4. Because laser ablation and vaporization processes can occur at a faster rate, smaller images ( $3 \times 3$  mm,  $256 \times 256$  pixels) were acquired to increase the acquisition rate to eight frames per second (125 ms per image). A small localized lesion of coagulated tissue is rapidly formed at 1 s. This is enlarged with vaporization and ejection of tissue occurring by 3 s. At 5 s, vacuolization of tissue due to rapid thermal effects is observed to the left of the ablation crater, and a deep carbonized crater has been formed at 8 s. Comparison with histology confirms the presence of vacuoles adjacent to the crater. However, the vacuoles created below the crater were not observed with OCT because of the shadowing effect from the carbonized tissue lining the crater wall.

## DISCUSSION

We have demonstrated the feasibility of using the high-resolution, real-time imaging capabilities of OCT for guiding resection of the prostate in a laboratory setting. Optical coherence tomography imaging has been used to track the dynamic changes of RF and laser ablation. In this study, real-time images were acquired at four frames per second ( $512 \times 256$  pixels) for RF ablation, and at eight frames per second ( $256 \times 256$  pixels) for laser ablation. These image acquisition rates were sufficient to track the changes that occurred during thermal ablation. Acquisition rates are inversely proportional to the number of pixels in the image. In this study, we have selected image sizes large

enough to visualize the entire ablation site while maximizing the acquisition rate. The image sequences of RF and laser ablation (Figs. 3 and 4) are representative examples of the use of OCT to guide a wide variety of resection techniques.

The images generated by OCT represent scanned areas several millimeters in size. Therefore, correlation with histology can be difficult for small regions of tissue and for small lesions. In addition, because the light source is near-infrared and invisible to the naked eye, positioning and marking of the tissue is difficult. The visible-light aiming beam (helium:neon, 632 nm) and tissue marking with India ink were essential to aid in determining the location of the section of tissue being scanned and registering these sites with corresponding histology. Tissue registration remains the primary limitation for comparing fine structures within OCT images with their corresponding histology, and becomes increasingly difficult at higher, cellular resolutions. The size of the scanned area is primarily limited by the beam-delivery mechanism. Because OCT is optic-based, and imaging can be performed through air, no index-matching medium is required between the device and the tissue, as in ultrasound. It is therefore possible to rapidly scan large areas of tissue.

The OCT image resolutions in the axial and transverse directions are independent. The axial resolution is inversely related to the bandwidth of the optical source. Therefore, superluminescent diodes and ultrafast solid-state lasers, which generated light with broad spectral bandwidths, provide higher axial imaging resolution. The transverse resolution is determined by Gaussian beam-focusing principles as in standard light microscopy. High transverse resolution can be achieved by tightly focusing the beam to a small spot. However, a trade-off exists in the form of subsequent reduction of the depth of field. The depth of field is the region of the focused optical beam where the transverse resolution remains relatively constant. Above (below) this region, the optical beam is converging (diverging) and the transverse resolution is less (larger beam size).

The OCT image resolutions used in this study ( $18 \mu\text{m}$  axial,  $30 \mu\text{m}$  transverse) are significantly higher than any existing clinical modality currently in use for imaging prostate ablation. The optical source used in this study was selected for its compact portable profile, high optical power for high-speed imaging, near-infrared wavelength for increased imaging penetration, and optical bandwidth for resolution. The transverse resolution was opti-

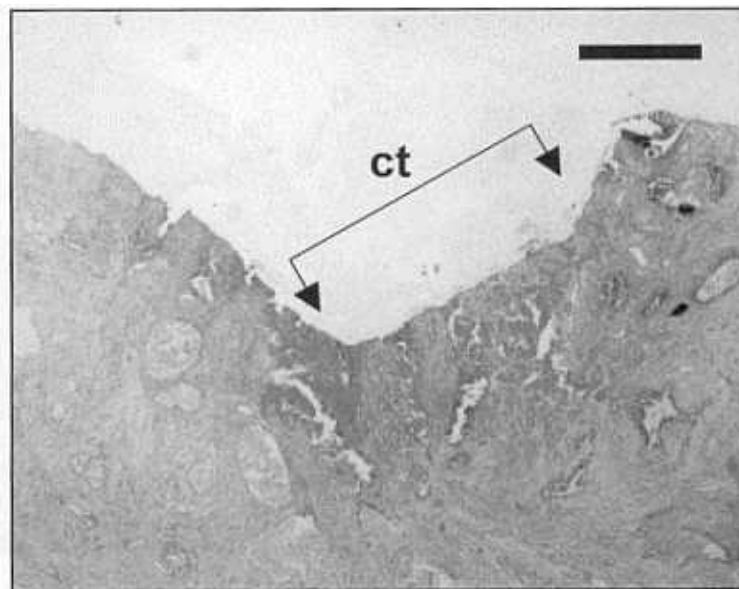
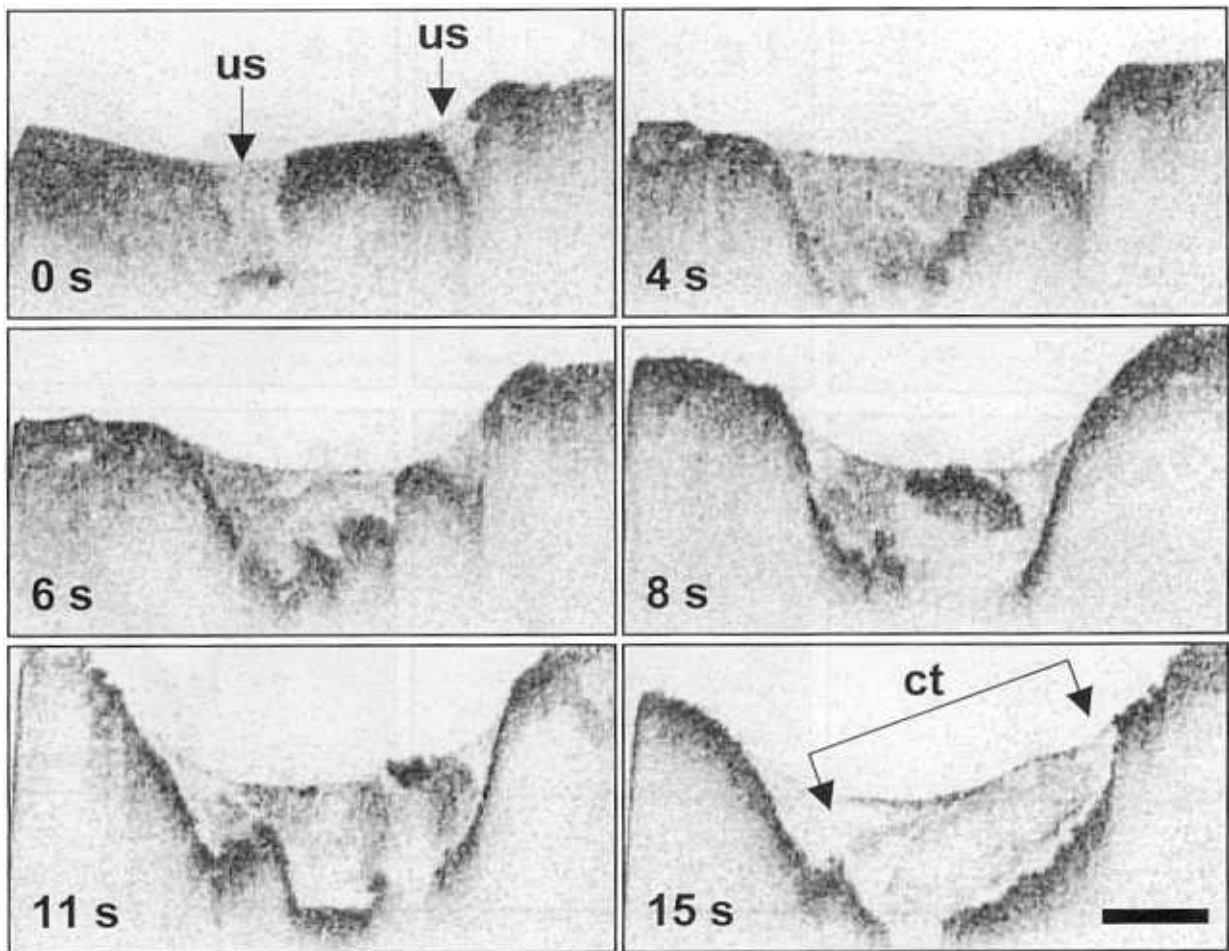


**Fig. 3.** Radiofrequency ablation. Image and video sequence demonstrating real-time OCT imaging of RF ablation of human prostate. 2 W RF power was delivered via a catheter tip for 15 s. The catheter tip was located immediately outside the OCT imaging plane to prevent a shadowing artifact. Prior to RF ablation (0 s), the OCT image reveals urethral sinuses (us) of the hemi-sectioned urethra filled with collections of saline. Arrows at 15 s and in the corresponding histology indicate the region of coagulated tissue (ct). Bar represents 1 mm.

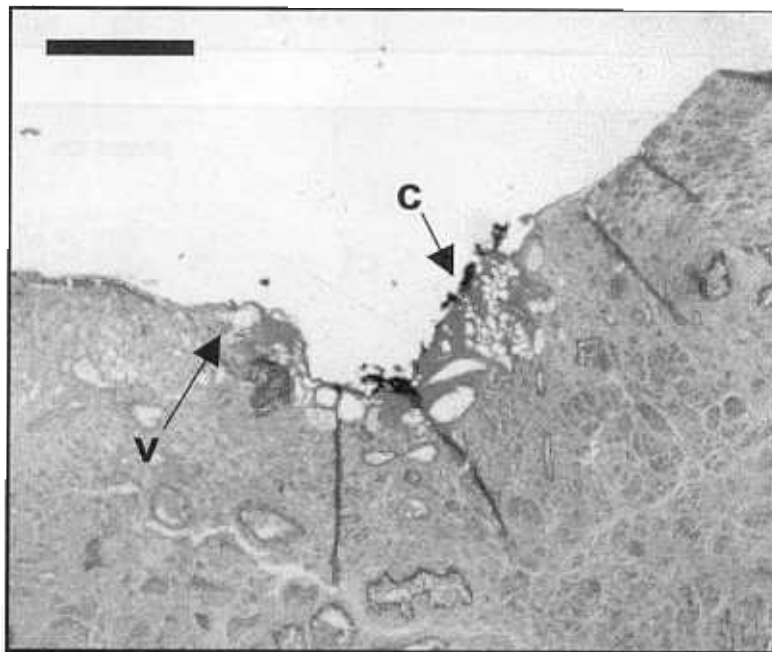
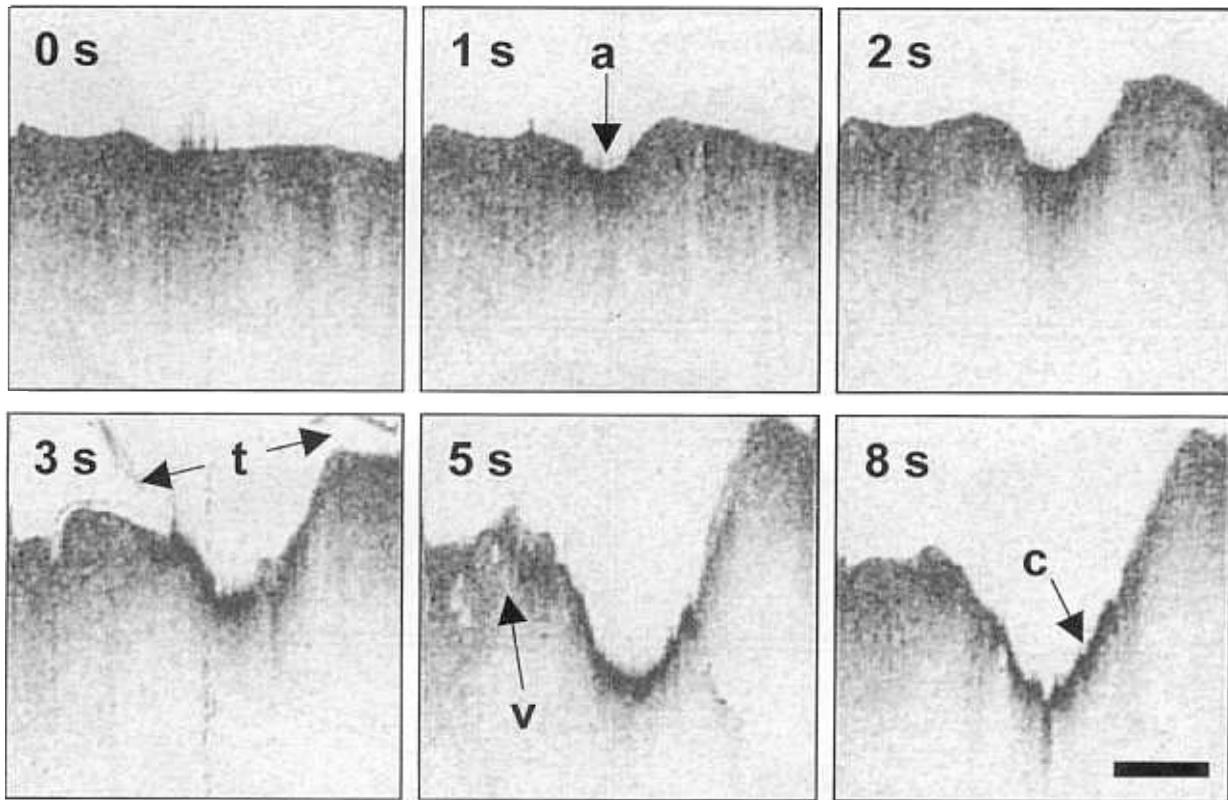


**Fig. 4.** Image and video sequence demonstrating real-time OCT imaging of argon laser ablation. 2 W argon power was delivered for 8 s. Localized ablation (a) began within 1 s, resulting in tissue disruption (t) at 3 s, vacuolization (v) of tissue along the outer margins at 5 s, and crater wall carbonization (c) at 8 s. The corresponding histology confirms the presence of vacuoles and carbonized tissue. Bar represents 1 mm.

mized to provide high transverse resolution and sufficient depth of field for imaging several millimeters into tissue. The resolutions used in this study were sufficient to image transurethral architectural prostate morphology, as well as to monitor thermal tissue changes that occurred during ablation. However, these resolutions were not sufficient to resolve small glands or individual cells (typically 10–30  $\mu\text{m}$ ). For the images shown in Figures 2–4, a single image pixel represents an area roughly the size of a single cell, making identification of cellular features improbable. Because of this, many images appear to be relatively homogeneous except when larger morphological structures are present. Previously, OCT has been used to image cell mitosis and migration in developmental biology animal models<sup>30</sup> and image resolutions as high as 1–2  $\mu\text{m}$  have been achieved using state-of-the-art laser systems.<sup>28,29</sup> However, the current size and complexity of these laser systems limit their use in a clinical setting.

OCT images display different features than histology because contrast in OCT images arises from differences in the optical backscattering of unresolvable cellular and subcellular components, rather than from staining as in histopathology. In Figures 2–4, high contrast exists between the *in vitro* tissue specimens and the surrounding saline solution. However, contrast within the tissue specimens is not as high, largely due to the loss of cell viability in these *in vitro* specimens, and to the image resolution being insufficient to identify cellular features. *In vivo* studies in animal and human subjects reveal images with significantly higher contrast in tissue.<sup>20,31</sup> *In vivo* imaging studies with advancements in OCT imaging resolution will further improve the ability to identify pathology intraoperatively based on microstructural or cellular differences between normal and pathologic tissue and cells.<sup>31</sup> The means by which OCT and histopathology represent tissue microstructure remains a central difference between these imaging modalities. However, the establishment of OCT image baselines for the interpretation of normal and abnormal morphologies in tissue will be a goal of future studies.

Compared to video endoscopic imaging that can only visualize surface features, OCT has the ability to image subsurface tissue architecture at micron-scale resolutions. OCT imaging penetration is largely dependent on scattering processes within tissue at near-infrared wavelengths. Therefore, tissues or cellular structures that are highly scattering will decrease the imaging penetration of the OCT

beam. For highly scattering tissue such as the human prostate, imaging penetration is typically 1–2 mm. There are two clinical conditions that will increase the scattering of the OCT beam and will likely reduce the ability to image subsurface features. First, the presence of blood will reduce imaging penetration. This was observed in an *in vivo* OCT imaging study of the rabbit aorta.<sup>32</sup> Imaging penetration, however, was improved by flushing the region being scanning with boluses of saline. A similar protocol will likely be necessary for *in vivo* imaging of prostate ablation. Second, rapid thermal ablation of tissue may produce a superficial layer of carbonized tissue as observed in Figure 4. This highly scattering tissue will produce a shadowing artifact, similar to what is observed in ultrasound, and reduce imaging penetration. Because tissue carbonization is undesirable for ablation, as well as for OCT imaging, clinical ablation protocols have been refined to limit the degree to which carbonization occurs.

This feasibility study used a microscope-based beam-delivery system to image *in vitro* human prostate specimens during laser and RF ablation. OCT catheter-based beam-delivery systems have been developed for *in vivo* applications.<sup>18,31</sup> A radial-imaging OCT catheter is one engineering design for a clinically viable beam-delivery device.<sup>30</sup> The small 1-mm diameter of the catheter can be readily passed through the urethra to the site of resection. This design collects optical backscatter from different radial positions and displays backscatter intensity in a polar coordinate (radial) image. One limitation of this design becomes evident with the presence of a resection device within the urethra, which may obscure the OCT imaging beam over a sector of the 360° scan range. This limitation can be overcome by the use of a linear reciprocating scan mechanism.<sup>31,33</sup> In this design, the OCT catheter components remain unchanged. Rather than rotating the catheter optics, they are translated in a reciprocal manner along the axis of the catheter and urethra. OCT images are subsequently displayed in a rectangular format. Because the OCT technology is optic based, there is also the potential to deliver both the imaging and ablation beams through the same instrument and optics.

The OCT instrument and catheter beam-delivery device are based on fiber optics, making the system compact and portable—approximately the size of an ultrasound cart. The technology utilizes components from the telecommunications industry. Therefore, the system is comparable in cost to ultrasound and relatively inexpensive compared to

imaging modalities such as CT and MRI. Unlike ultrasound probes and catheters, no active transducer is necessary within a catheter-based beam-delivery device. Hence, OCT catheters can be inexpensive and disposable.

In this study, the feasibility of using OCT for the real-time imaging of prostate ablation has been demonstrated. Using the OCT technology, an image-based comparison was made between the real-time dynamics of radiofrequency and laser ablation of *in vitro* prostate specimens in a laboratory setting. In addition to demonstrating surgical image guidance, OCT provides insight into the mechanisms of tissue damage, and permits high-speed, high-resolution subsurface imaging of the ablation process. Future studies will investigate minimally invasive techniques for imaging the prostate *in vivo* using OCT. Integration of minimally invasive catheter-based OCT image guidance with surgical ablation techniques may have the potential to intraoperatively monitor and provide dosimetric feedback during prostate resection.

#### ACKNOWLEDGMENT

We would like to thank Dr. David Keane from the Massachusetts General Hospital for his assistance with the operation of the radiofrequency ablation equipment, and Christine Jesser for her contributions in the laboratory. We would like to acknowledge former group members, Drs. Brett Bouma and Gary Tearney, currently at the Wellman Laboratory of Photomedicine, Massachusetts General Hospital, for their assistance. This research is sponsored in part by the National Institutes of Health, Contracts NIH-9-R01-EY11289-13 (J.G.F.), NIH-1-R01-CA75289-03 (J.G.F. and M.E.B.), 1R01AR44812-02 (M.E.B.), and NIH-1-R29-HL55686-01A1 (M.E.B.); the Medical Free Electron Laser Program, Office of Naval Research, Contract N00014-94-1-0717 (J.G.F. and M.E.B.); the Whitaker Foundation, Contract 96-0205 (M.E.B.); and the Air Force Palace Knight Program (S.A.B.).

#### REFERENCES

1. Horninger W, Janetschek G, Watson G, Reissigl A, Strasser H, Bartsch G. Are contact laser, interstitial laser, and transurethral ultrasound-guided laser-induced prostatectomy superior to transurethral prostatectomy? *Prostate* 1997;31:255–263.
2. Keoghane SR, Lawrence KC, Gray AM, Doll HA, Hancock AM, Turner K, Sullivan ME, Dyar O, Cranston D. A double-blind randomized controlled trial and economic evaluation of transurethral resection vs contact laser vaporization for benign prostatic enlargement: A 3-year follow-up. *Br J Urol Int* 2000;85:74–78.
3. Shingleton WB, Terrell F, Renfro DL, Kolski JM, Fowler JE Jr. A randomized prospective study of laser ablation of the prostate versus transurethral resection of the prostate in men with benign prostatic hyperplasia. *Urology* 1999;54:1017–1021.
4. Hegarty NJ, Fitzpatrick JM. High intensity focused ultrasound in benign prostatic hyperplasia. *Eur J Ultrasound* 1999;9:55–60.
5. Mulligan ED, Lynch TH, Mulvin D, Greene D, Smith JM, Fitzpatrick JM. High-intensity focused ultrasound in the treatment of benign prostatic hyperplasia. *Br J Urol* 1997;79:177–180.
6. Nawrocki JD, Bell TJ, Lawrence WT, Ward JP. A randomized controlled trial of transurethral microwave thermotherapy. *Br J Urol* 1997;79:389–393.
7. Thalmann GN, Graber SF, Bitton A, Burkhard FC, Gruenig O, Studer UE. Transurethral thermotherapy for benign prostatic hyperplasia significantly decreases infravesical obstruction: Results in 134 patients after 1 year. *J Urol* 1999;162:387–393.
8. Gilling PJ, Cass CB, Malcolm A, Cresswell M, Fraundorfer MR, Kabalin JN. Holmium laser resection of the prostate versus neodymium:yttrium-aluminum-garnet visual laser ablation of the prostate: A randomized prospective comparison of two techniques for laser prostatectomy. *Urology* 1998;51:573–577.
9. Matsuoka K, Iida S, Tomiyasu K, Shimada A, Noda S. Transurethral holmium laser resection of the prostate. *J Urol* 2000;163:515–518.
10. Dimitri M. TURP with the new superpulsed radiofrequency energy: More than a gold standard. *Eur Urol* 1999;36:331–334.
11. Namiki K, Shiozawa H, Tsuzuki M, Mamiya Y, Matsumoto T, Miki M. Efficacy of transurethral needle ablation of the prostate for the treatment of benign prostatic hyperplasia. *Int J Urol* 1999;6:341–345.
12. Liney GP, Turnbull LW, Knowles AJ. In vivo magnetic resonance spectroscopy and dynamic contrast enhanced imaging of the prostate gland. *NMR Biomed* 1999;12:39–44.
13. Mueller-Lisse UG, Thoma M, Faber S, Heuck AF, Muschter R, Schneede P, Weninger E, Hofstetter AG, Reiser MF. Coagulative interstitial laser-induced thermotherapy of benign prostatic hyperplasia: Online imaging with a T2-weighted fast spin-echo MR sequence—experience in six patients. *Radiology* 1999;210:373–379.
14. Boppart SA, Herrmann J, Pitris C, Stamper DL, Brezinski ME, Fujimoto JG. High-resolution optical coherence tomography-guided laser ablation of surgical tissue. *J Surg Res* 1999; 82:275–284.
15. Brezinski ME, Tearney GJ, Boppart SA, Swanson EA, Southern JF, Fujimoto JG. Optical biopsy with optical coherence tomography: Feasibility for surgical diagnostics. *J Surg Res* 1997;71:32–40.
16. Huang D, Swanson EA, Lin CP, Schuman JS, Stinson

- WG, Chang W, Hee MR, Flotte T, Gregory K, Puliafito CA, Fujimoto JG. Optical coherence tomography. *Science* 1991;254:1178–1180.
17. Boppart SA, Bouma BE, Pitris C, Tearney GJ, Southern JF, Brezinski ME, Fujimoto JG. Intraoperative assessment of microsurgery with three-dimensional optical coherence tomography. *Radiology* 1998;208:81–86.
  18. Sergeev AM, Gelikonov VM, Gelikonov GV, Feldchtein FI, Kuranov RV, Gladkova ND, Shakhova NM, Snopova LB, Shakov AV, Kuznetzova IA, Denisenko AN, Pochinko VV, Chumakov YP, Streltsova OS. In vivo endoscopic OCT imaging of precancer and cancer states of human mucosa. *Opt Express* 1997;1:432–440.
  19. Boppart SA, Bouma BE, Pitris C, Tearney GJ, Brezinski ME, Fujimoto JG. Forward-imaging instruments for optical coherence tomography imaging. *Opt Lett* 1997;22:1618–1620.
  20. Tearney GJ, Boppart SA, Bouma BE, Brezinski ME, Weissman NJ, Southern JF, Fujimoto JG. Scanning single-mode fiber optic catheter-endoscope for optical coherence tomography. *Opt Lett* 1996;21:543–545.
  21. Brezinski ME, Tearney GJ, Bouma BE, Izatt JA, Hee MR, Swanson EA, Southern JF, Fujimoto JG. Optical coherence tomography for optical biopsy: Properties and demonstration of vascular pathology. *Circulation* 1996;93:1206–1213.
  22. Schmitt JM, Yadlowsky M, Bonner RF. Subsurface imaging of living skin with optical coherence microscopy. *Dermatology* 1995;191:93–98.
  23. Rollins AM, Ung-arunyawee R, Chak A, Wong RCK, Kobayashi K, Sivak MV Jr, Izatt JA. Real-time in vivo imaging of human gastrointestinal ultrastructure by use of endoscopic optical coherence tomography with a novel efficient interferometer design. *Opt Lett* 1999;24:1358–1360.
  24. Tearney GJ, Brezinski ME, Bouma BE, Boppart SA, Pitris C, Southern JF, Fujimoto JG. In vivo endoscopic optical biopsy with optical coherence tomography. *Science* 1997;276:2037–2039.
  25. Tearney GJ, Brezinski ME, Southern JF, Bouma BE, Boppart SA, Fujimoto JG. Optical biopsy in human urologic tissue using optical coherence tomography. *J Urol* 1997;157:1915–1919.
  26. Fercher AF, Mengedocht K, Werner W. Eye-length measurement by interferometry with partially coherent light. *Opt Lett* 1988;13:186–188.
  27. Takada K, Yokohama I, Chida K, Noda J. New measurement system for fault location in optical waveguide devices based on an interferometric technique. *Appl Opt* 1987;26:1603–1608.
  28. Clivaz S, Marquis-Weible F, Salathe RP, Novak RP, Gilgen HH. High-resolution reflectometry in biological tissues. *Opt Lett* 1992;17:4–6.
  29. Drexler W, Morgner U, Kartner FX, Pitris C, Boppart SA, Li X, Ippen EP, Fujimoto JG. In vivo ultrahigh resolution optical coherence tomography. *Opt Lett* 1999;24:1221–1223.
  30. Boppart SA, Bouma BE, Pitris C, Southern JF, Brezinski ME, Fujimoto JG. In vivo cellular optical coherence tomography imaging. *Nat Med* 1998;4:861–865.
  31. Li X, Boppart SA, Van Dam J, Mashimo H, Mutinga M, Drexler W, Klein M, Pitris C, Krinsky ML, Brezinski ME, Fujimoto JG. Optical coherence tomography: Advanced technology for the endoscopic imaging of Barrett's esophagus. *Endoscopy* 2000;32:921–930. *Endoscopy* 2000;32:921–930.
  32. Fujimoto JG, Boppart SA, Tearney GJ, Bouma BE, Pitris C, Brezinski ME. High-resolution in vivo intra-arterial imaging with optical coherence tomography. *Heart* 1999;82:128–133.
  33. Bouma BE, Tearney GJ. Power-efficient nonreciprocal interferometer and linear-scanning fiber-optic catheter for optical coherence tomography. *Opt Lett* 1999;24:531–533.